VIBRATION CHARACTERISTICS OF THE HPOTP
(High Pressure Oxygen Turbopump)
OF THE SSME
(Space Shuttle Main Engine)[1]

Dara W. Childs, Professor
David S. Moyer, Graduate Research Assistant
Mechanical Engineering Department
Texas A&M University
College Station, Texas 77843

Abstract

A review is presented of various rotordynamic problems which have been encountered and eliminated in developing the current flight engines, and continuing subsynchronous problems which are being encountered in developing a 109% power level engine. The basic model for the HPOTP including the structural dynamic model for the rotor and housing and component models for the liquid and gas seals, turbine-clearance excitation forces, and impeller-diffuser forces are discussed. Results from a linear model are used to examine the synchronous response and stability characteristics of the HPOTP, examining bearing load and stability problems associated with the second critical speed. Various seal modifications are examined and shown to have favorable consequences with respect to bearing reactions and stability. Difference between linear and nonlinear model results are discussed and explained in terms of simple models.

The transient nonlinear model is used to demonstrate forced subsynchronous motion similar to that observed in test data for models which are lightly damped but stable. The subsynchronous motion

results from bearing clearance nonlinearities.
Simulation results indicate that synchronous bearing
loads can be reduced but that subsynchronous motion
is not eliminated by seal modifications alone.

INTRODUCTION

The SSME (Space Shuttle Main Engine) has been
under development by Rocketdyne Division of Rockwell
International since the early 1970's. The George C.
Marshall Space Flight Center has administered the
program development for NASA. The SSME is designed
to operate at the following three conditions:

MPL (Minimum Power Level); ω = 20,900 cpm
RPL (Rated Power Level); ω = 28,200 cpm
FPL (Full Power Level); ω = 30,380 cpm

At RPL the turbines develop approximately 1.71 X 10^7
watts (22,900 Hp). FPL is 109% of RPL. RPL
performance is adequate for the equatorial orbits
which have been flown to date; however, polar orbits
require FPL performance. This paper concerns various
rotordynamics problems related to the HPOTP (High
Pressure Oxygen Turbopump) which were eliminated in
developing a reliable RPL engine and new problems
which are being encountered in developing FPL
performance.

As compared to more conventional turbomachinery,
liquid-rocket-engine turbopumps present the
following distinctive rotordynamics development
problems:

(a) The units operate in ball bearings which are
    lubricated with the cryogenic fluid being
    pumped. The bearings themselves provide
    virtually no damping.
(b) Because of the extraordinarily low viscosity
    of liquid oxygen and liquid hydrogen, neither
    fluid can be effectively used in a
    squeeze-film damper. Moreover, the presence
    of these cryogenic fluids precludes the use

of other fluids in conventional dampers or elastomeric dampers.

(c) Oxygen-compatible motion transducers are under development; however, they are not currently available. Moreover, a typical turbopump design presents severe difficulty in access to the rotating assembly for relative motion measurements; particularly, when access for motion measurements was not a consideration in the initial design. Vibration data for the SSME turbopumps has largely been confined to the output of accelerometers mounted on the housing. For most of the development period of the HPOTP, there has been no speed probe pickup and no once-per-revolution phase mark from the shaft to use in data analysis.

The calculated linear critical speeds for the current nominal HPOTP are at approximately 12,500 cpm (208 Hz) and 32,500 cpm (540 Hz). These calculated values are for complete housing-rotor models including seals, clearance-excitation forces, gyroscopic coupling, etc. The arrangement of the high pressure turbopumps in the powerhead are illustrated in figure 1. The HPOTP rotating assembly is illustrated in figure 2. The undamped, zero-running-speed, rotor-housing modes associated with the first and second critical speeds are illustrated in figure 3. The modeshape associated with the first critical speed primarily involves overhung motion of the turbine with relatively small amplitudes at the bearings and main impeller. The modeshape associated with the second critical speed involves large amplitudes at the main impeller and bearings with small amplitudes at the turbine.

Initial vibration problems with the HPOTP involved motion associated with the first critical speed. Synchronous and subsynchronous (at approximately 200 Hz) motion was excessive. This problem was remedied by changing the turbine

454

interstage seal from a stepped-labyrinth configuraton to a convergent taper seal with a honeycomb stator and a smooth rotor. This change was implemented based on the beneficial consequences of a similar change in the pump interstage seals of the HPFTP (High Pressure Fuel Turbopump) [1].

The second problem associated with the HPTOP involved subsynchronous vibrations at approximately 400-420 Hz. This motion tended to initiate when the running speed reached approximately 400 Hz, and persisted as subsynchronous motion when the running speed was increased. A failure and explosion of the HPOTP occurred in a test run when the running speed first traversed the maximum-amplitude frequency range and then was reduced to and remained at the now synchronous frequency. The failure was attributed to an inadequate bearing-carrier design which caused unequal load sharing of the bearings. Subsequently, redesigned bearing carriers eliminated the "400 Hz" subsynchronous motion. The general feeling was that the new bearing carrier designs caused a more equal load sharing and maintained the correct axial bearing preloads, thus realizing the "expected" radial stiffness of the bearings and elevated the rotor second critical speed.

The bearing-carrier redesign was sufficient to yield a reliable pump for RPL operations; however, demonstration of FPL capability has been impeded by repeated occurrence of subsynchronous motion in the 450-500 Hz frequency range. The incidence of this motion rarely occurs during initial operation at higher power levels, but tends to develop after an accumulation of time and develops more rapidly with higher synchronous vibration levels. However, once a unit begins to "whirl", it will repeatedly whirl, generally with progressively increasing severity. The frequency of the subsynchronous motion is sometimes at a fixed fraction of running speed ranging from 88 to 95%. This "tracking" characteristic is in marked contrast to the earlier "400 Hz" phenomenon where the whirl-frequency of the

subsynchronous motion remained constant, relatively independent of running speed.

Post-run inspection of turbopumps has revealed that, although the balls in some bearings, primarily bearing 2, appear to be unblemished, their diameters have in fact, been reduced by as much as 0.17 mm in some cases. The cause of this dimensional attrition is unknown, but has been ascribed to either excessive radial loads or the absence of radial loads which leads to skidding.

The analysis results which have been completed to date and are reported herein do not provide a complete or comprehensive explanation for the measured dynamic characteristics of the HPOTP; however, they do provide answers for the following questions:

(a) What are the linear dynamic characteristics of the <u>nominal</u> turbopump model ith respect to critical-speed locations, bearing reactions, predicted housing accelerometer levels, and predicted onset speeds of instability?

(b) How can the linear dynamic characteristics be improved by feasible, physical modification of the HPOTP seals?

(c) What causes the subsynchronous motion?

(d) From a rotodynamics viewpoint, what are the principal problems experienced by the HPOTP?

(e) What improvements are possible with the HPOTP?

The following section briefly describes the structure and components of the rotordynamic model, with the succeeding section describing the results of linear and nonlinear analysis.

THE ROTORDYNAMICS MODEL

<u>Structural Dynamics Model.</u>   The structural-dynamics model of the rotor and the housing form the

basic framework of the turbopump model. Both the
housing and *rotor* structural dynamics models used
here were developed by Rocketdyne. A general
three-dimensional finite-element approach was used to
model the HPOTP housing without the *rotor*. A lumped
parameter model was developed for the rotor using
beam structural elements and lumped masses and
inertias. The *rotordynamics* model uses modes from
the housing model (without the rotor) and free-free
rotor modes.

Bearings. The bearings are the structural
elements which tie the rotors and housing together.
As illustrated in figure 2, there are two sets of
bearings. The net load from each set is transmitted
through a plate-cylinder structure to the housing.
The bearings in a bearing set are axially preloaded
against each other, but are not designed to accept
axial thrust loads from the turbopumps. A
balance-piston arrangement at the discharge of the
main impeller absorbs axial thrust, and radial
clearances are provided at the bearing outer faces to
allow the bearings to slip axially without developing
excessive axial loads.
Experience and limited test data [2] for the
SSME bearings indicate a nominal *stiffness* of
approximately 8.76 X 10^7 N/m. This is approximately
one half of the values predicted by A. B. Jones-based
analysis [3].
The radial clearances provided at the bearings
to permit axial motion provides an essential
"dead-band" nonlinearity. The clearance values used
in this study are

$$\delta_P = 0.0127 \text{ mm}, \ \delta_T = 0.0127 \text{mm} \hspace{2em} (1)$$

where P and T denote pump and turbine bearings.

Liquid Seals. Liquid wear-ring seals are
provided at the inlet and discharge of the boost
impeller. The current inlet seal is a stepped
labyrinth design with four cavities. The current

discharge seal is a three segment, stepped seal.
Each constant-radius seal segment has a series of
circumferential grooves.

Experience and limited test data [3] have shown
that labyrinth or serrated seals of the type
currently employed on the impeller inlet and
discharge yield stiffness and damping coefficients
which are substantially smaller than corresponding
values for smooth constant clearance seals.
Replacing the current grooved boost-impeller
wear-ring seals with plain annular seals has the
potential for a beneficial increase in stiffness and
damping in the HPOTP. In fact, as the following
discussion explains, various additional possibilities
exist for optimizing seals.

The force-motion model for liquid seals has the
form

$$
- \begin{Bmatrix} F_X \\ F_Y \end{Bmatrix} = \begin{bmatrix} K & k \\ -k & K \end{bmatrix} \begin{Bmatrix} X \\ Y \end{Bmatrix} + \begin{bmatrix} C & c \\ -c & C \end{bmatrix} \begin{Bmatrix} \dot{X} \\ \dot{Y} \end{Bmatrix} + \begin{bmatrix} M & m \\ -m & M \end{bmatrix} \begin{Bmatrix} \ddot{X} \\ \ddot{Y} \end{Bmatrix}
$$

In this model (X, Y) are the components of the
relative motion between the rotor and housing.
Black, et al. [5, 6] were responsible for most of the
analytical developments related to the analysis of
seals leading to the definition of stiffness,
damping, and added-mass coefficients. His analysis
demonstrates that the "cross-coupled" stiffness
coefficient, k, arises solely due to fluid rotation
within the seal. As a fluid element proceeds axially
along an annular seal, shear forces at the rotor
accelerate or decelerate the fluid tangentially until
an asymptotic value is reached. For a seal with the
same directionally-homogeneous surface-roughness
treatment on the rotor and the housing, the average
asymtotic tangential velocity is $R\omega/2$ where R is the
seal radius and ω is the rotor running speed.

The cross-coupled stiffness coefficient k acts
in opposition to the direct damping coefficient C to
destabilize rotors. Hence, steps which can be taken

to reduce the net fluid rotation within a seal will improve stability by reducing k. The following two steps are currently under consideration for providing more net damping to the HPOTP rotating assembly:

(a) If the _inlet_ tangential velocity can be reduced, the high axial velocities in a cryogenic seal are such that the fluid may proceed through a seal without substantially increasing its tangential velocity. An antivortex web has been proposed at the inlet to the boost-impeller inlet seal to reduce the inlet tangential velocity and yield a reduced k. This practice has been followed previously for the labyrinth seals of high pressure compressors.

(b) Von Pragenau [7] has recently demonstrated that the asymptotic tangential velocity can be modified if a different surface roughness is used for the rotor and stator elements. Rough rotor/smooth stator and smooth rotor/rough stator combinations yield higher and lower asymptotic values, respectively. Von Pragenau calls the rough stator/smooth rotor configuration a "damper seal" because of its enhanced stability characteristics. The roughness has the additional potential benefit of reducing leakage. Damper seal configurations are presently under consideration for both the inlet and discharge seals of the boost impeller.

Liquid seal coefficients for the boost impeller seals were calculated based on analysis by Childs and Kim [8]. Current analyses yield finite-length solutions for constant-clearance or convergent-tapered seals with different but directionally-homogeneous surface roughness treatments on the rotor and stator.

Gas Seals. The HPOTP turbines are shrouded, and single-cavity tip seals are provided to reduce

leakage between the turbine shroud and the stator. The interstage seal between the turbines uses a honeycomb stator element with a smooth rotor and inlet anti-vortex ribs to reduce the inlet tangential velocity component. A floating-ring shaft seal is provided at the turbine discharge to restrict leakage of the hot turbine gases towards the lox within the pump. The flow across this seal is choked.

Seal coefficients calculations used in the study are based on the analyses of Nelson [9]. The analyses apply to constant-clearance or convergent taper geometries, account for the development of tangential velocity within the seals, and different but directionally-homogeneous surface roughness on the rotor and stator.

Turbine Clearance Excitation Forces. Clearance excitation forces are developed by turbines due to the dependency of local efficiency on local clearances. The destabilizing force is modeled by

$$\begin{Bmatrix} F_X \\ F_Y \end{Bmatrix} = \begin{bmatrix} 0 & k_T \\ -k_T & 0 \end{bmatrix} \begin{Bmatrix} X \\ Y \end{Bmatrix} ; \quad k_T = \frac{\beta T}{D_p H} \qquad (3)$$

where T is the turbine torque, D_p is the average pitch diameter of the turbine blades, H is the average height, and β defines the change in turbine efficiency due to uniform changes in clearance. Again, the components (X, Y) of Eq. (3) define the displacement of the turbine relative to the housing. Thomas initially identified this destablizing phenomenon [10], while Alford [11] subsequently and independently developed the same model. Test results for shrouded turbines have yielded values for β on the order of 0.6 [12].

Impeller-Diffuser Forces. A test program has been under way at the California Institute of Technology for some time to measure the static and dynamic forces experienced by a pump impeller in either a volute or a vaned diffuser. Chamieh et al.

460

[13] have defined the following model on the basis of static measurements of an impeller within a vaned diffuser:

$$-\frac{1}{\rho A_2 V_2^2} \begin{Bmatrix} F_X \\ F_Y \end{Bmatrix} = \begin{bmatrix} K* & k* \\ -k* & K* \end{bmatrix} \begin{Bmatrix} X/R_2 \\ Y/R_2 \end{Bmatrix} = \begin{bmatrix} -2.0 & 0.7 \\ -0.7 & -2.0 \end{bmatrix} \begin{Bmatrix} X/R_2 \\ Y/R_2 \end{Bmatrix} \quad (4)$$

where R_2 is the impeller radius, ρ is the fluid density, $V_2 = R_2\omega$ is the impeller tip velocity, and $A_2 = 2\pi R_2 b_2$ is the exit flow area. Note that the direct-stiffness coefficient in Eq. (4) is negative, i.e., the impeller-diffuser force causes a reduction in rotor stiffness. From Eq. (4), the dimensional impeller-diffuser coefficients are defined by

$$\overline{K} = K* \frac{\rho A_2 V_2^2}{2R_2} = K* (\pi \rho b_2 R_2^2)\omega^2$$

$$\overline{k} = k*(\pi \rho b_2 R_2^2)\omega^2 \quad (5)$$

ANALYSIS PROCEDURES AND RESULTS

Introduction

The radial clearances which are provided at the outer races of the bearings to permit axial slipping and prevent the bearings from absorbing axial loads provide the essential nonlinearity in a rotordynamics model for the HPOTP. If these "dead band" clearances are eliminated, the resultant model is basically linear. As the following sections demonstrates, the results of linear and nonlinear analysis differ substantially, but linear analysis remains an efficient procedure for general characterization of the turbopump's rotordynamics.

Linear Analysis Procedure and Results
Rotordynamic Characteristics of the Nominal Model

The analysis procedure used here is basically the same as that outlined in reference [1]. Modal

461

coordinates based on the zero-running-speed coupled rotor-housing mode are used. Gyroscopic coupling and forces due to seals, turbine clearance-excitation, the interaction of impellers and diffusers, damping, etc., couple the modal coordinates via modal stiffness, damping, and inertial matrices. The onset speed of instability for a turbopump configuration is defined by calculating the complex eigenvalues of the system dynamic matrix at various speeds. Synchronous-response amplitudes of bearing reactions and acceleration levels of accelerometers mounted on the turbopump housing due to imbalance are calculated.

For the purposes of the present discussion, the nominal linear model is defined as having bearing stiffness on the order of 8.76×10^7 N/m ($.5 \times 10^6$ lbs/in). Calculated seal coefficients are based on the dimensions of seals currently used in the turbopump. The clearance-excitation force coefficient at the turbines use a β of 0.4.

An inspection of the modeshapes of figure 3 indicates that the clearance-excitation force at the turbine represents the dominant destabilizing excitation force for motion associated with the first critical speed. Following the initial "400 Hz" subsynchronous vibration problem, the suggestion was made [15] that impeller-diffuser-interaction forces provided the principal destablizing mechanism for motion associated with the second critical speed. The published cross-coupling coefficients of Eq. (4) certainly supported this view. If the nominal model includes the stiffness coefficients of Eq. (4), the OSI (Onset Speed of Instability) is only 17,200 cpm. However, the stability is very sensitive to damping, and the additional 875 Ns/m (5.0 lb sec/in) at the main impeller with no bearing damping elevates the OSI to 30,480 cpm. The whirl frequency at OSI is 536 Hz. This concentrated damping coefficient acts to restrain relative motion between the rotor and housing, and is used in the nominal linear model.

Figure 4 illustrates the bearing reaction for running speeds from 5,000 to 40,000 cpm. The first

and second critical speeds are evident, with the
second critical speed clearly having little or no
damping. Figure 5(a) illustrates the same results
for speeds from 5,000 cpm to FPL. Figures 5(b) and
(c) illustrate predicted acceleration levels for
accelerometers mounted on the housing at the pump and
turbine ends of the turbopump. Clearly, FPL is quite
near the predicted second critical speed. Also,
while the bearing reactions are responsive to the
"rotor" critical speeds, the housing accelerometer
levels may respond more sharply to rotor-housing
combined modes. This is particularly true for the
first critical speed at approximately 12,500 rpm
However, the predicted accelerometer levels are quite
responsive to motion associated with the "rotor"
second critical speed at approximately 32,500 cpm.

   (a) Response. The proximity of the second
       critical speed to FPL is a continuing cause
       for concern with respect to excessive bearing
       loads. Even modest losses of bearing
       stiffnesses are sufficient to drop the second
       critical speed into the operating range.
   (b) Stability. Based on the prior "400 Hz"
       experience with this turbopump, the second
       critical speed appears to be lightly damped
       and subject to instability.

**Seal Modifications to Improve Rotordynamic Response
and Stability**
     The preceding material demonstrated the relevant
dynamic characteristics of the HPOTP with respect to
response and stability. The present section deals
with predicted improvements in rotordynamic response
due to the following seal modifications:

   (a) Replace the current inlet and discharge seals
       of the boost impeller with "damper" seals
       using a rough stator and smooth rotor. Test
       results at Texas A&M University of proposed
       damper seal and smooth seals flight
       candidates show a substantial reduction in

leakage due to roughness and slight increases in direct stiffnesses and net damping [8].

(b) Replace the current unshrouded impeller with shrouded impellers and use the outer surfaces of the shrouded impeller to develop seal forces.

Figure 6 illustrates the bearing reactions which result for choice (a), and a comparison of this result with the nominal-model results of figure 5 (a) indicates a sharp reduction in bearing reactions. Moreover, the OSI is increased moderately. Table 1 provides a summary of the results for both the nominal configuration and the seal modifications cited above and demonstrates that the damper seals yield a predicted reduction in bearing loads on the order of 37% and an increase of the predicted OSI to 36,350 rpm.

CONFIGURATION	OSI (cpm)	WHIRL FREQ. (Hz)	BEARING REACTIONS at FPL (lbs)			
			1	2	3	4
Nominal	30,480	536	553	635	667	548
Nominal with With Boost-Impeller Seals	36,350	576	251	349	513	411
Nominal with Shrouded-Inducer Seal	59,950	315	80	85	57	58

Table 1. Linear OSI, whirl frequency, and predicted bearing reactions at FPL.

Figure 7 illustrates the results for the shrouded inducer configuration. Stated briefly, the second critical speed is simply eliminated for this configuration, and OSI is much greater than FPL.

An assessment of the results presented in figures 6, 7, and table 1 supports the following general conclusions:

464

(a) Modification of the boost impeller seals has
    the potential for significantly reducing
    bearing reactions at FPL as compared to the
    nominal model. However, the second critical
    speed remains only slightly above FPL and any
    loss of bearing stiffness will drop it into
    the operating range.
(b) The damper-seal modification yields a
    predicted increase of the OSI by 19%.
(c) The shrouded-inducer design eliminates both
    the second critical speed and the stability
    problem.

Nonlinear Analysis Procedures and Results

As noted previously, the bearing "dead-band"
clearances provide the essential nonlinearity in the
HPOTP model. The bearing clearances interact with
the effects of side loads and rotor imbalance to
yield significantly different results for a nonlinear
model than those predicted by linear models.

Figure 8 illustrates the analytical model used
by Yamamoto [14] to investigate the influence of
bearing clearances on rotordynamic response in the
absence of side loads. For zero bearing clearances,
the model of figure 8 reduces to a simple Jeffcott
model with viscous external damping. Figure 9
illustrates the response characteristics for a
progressive increase in the ratio of bearing
clearance to imbalance eccentricity $\hat{e} = e/a$. The
results are for a damping ratio of 2.5%, and indicate
the speed location of maximum bearing reactions is
reduced by increasing $\hat{e}$. Moreover, the drop in
amplitude for speeds above the maximum bearing-load
can be preciptious. The response characteristics of
figure 9 can give rise to "jump" phenomena with the
synchronous vibration level jumping either up or down
for very small changes in running speed. Flight
data for the HPOTP have demonstrated sudden step
increases in accelerometer levels.

From these results, one would anticipate that
bearing clearances could easily drop the
peak-bearing-load running speed location associated

465

with the second critical speed into the operating range. In fact, parametric studies of the bearing clearances clearly confirm this result [15]. They also confirm that peak-bearing-load speeds can be reduced below FPL for sufficiently large clearances. Hence for a given running speed, a nonlinear model with bearing clearances can yield either substantially larger or smaller bearing reactions than the linear model.

The nonlinear model was verified by comparison to results from the linear model, e.g., the second-critical-speed location at 32,500 cpm was obtained for zero bearing clearances. Figure 10 illustrates the bearing 2 reaction magnitude and turbine acceleration signals at FPL for the nominal model with the bearing clearances of Eq. (1). Observe the "clipping" of the bearing reaction magnitudes in figure 10 (a), which results from motion through the bearing deadband. Motion in and out of the deadband results as a combination of static displacement due to the impeller and turbine side loads and elliptical orbits due to imbalance. Bearing clipping generates a nearly periodic impulsive loading at the bearing that excites the beating motion which is evident in the accelerometer signal prediction of figure 10 (b). Spectrum analysis results of the accelerometer signals at FPL and two higher speeds are provided in figure 11 and reveal a subsynchronous signal at 26,500 cpm (443 Hz). Both the synchronous and subsynchronous signals are observed to decrease as the running speed increases. Observe that the frequency of the subsynchronous motion is consistent with frequencies observed in test data as opposed to the linear predictions of 520 Hz. The linear model corresponding to the result of figure 10 is lightly damped but stable. The nonlinear model remains in a limit cycle motion with subsynchronous components until the destabilizing force components at the main impeller are increased to 250% of their nominal values, but then diverge exponentially. Based on these observations, the subsynchronous component of figure 11 is deemed to be the result of bearing

466

nonlinearities and not the result of an instability. However, the nonlinear subharmonic motion can only be developed for light rotor damping.

The subsynchronous motion of figures 10 and 11 arises at speeds above the maximum synchronous response speed predicted by Yamamoto's model in figure 9. This statement is supported by the results in figure 12 which shows the bearing 2 reaction magnitude predictions at 29,450 cpm.

A second nonlinear model configuration which yielded a substantial subsynchronous vibration component was obtained by doubling both the imbalance magnitudes and the destabilizing force coefficients at the main impeller, adding damping at the bearing (350 Ns/m or 2 lb s/in), and increasing the damping at the main impeller to 2625 Ns/m (15 lb s/in). This configuration is predicted to be linearly stable at FPL. Spectral analysis results for this configuration at FPL and two higher speeds are presented figure 12. In this case, the subsynchronous component increases with running speed, while the synchronous component decreases.

The response characteristics of a nonlinear model including bearing clearances is sensitive to many parameters including bearing clearances, imbalance magnitudes, side load magnitudes, damping coefficients, destabilizing force magnitudes, etc., and a study including a systematic variation of all these parameter would be helpful. However, the simulation results of figures 10 through 12 are sufficient to support the following conclusions:

(a) The subsynchronous motion which is evident in these results can be obtained due to bearing-clearance nonlinearies for a linearly-stable but lightly damped model.

(b) A whirl frequency of subsynchronous motion at 440 Hz is predicted by the nonlinear model as compared to 520 Hz for the linear model. This whirl frequency reduction results solely from the bearing clearances, and does not require any stiffness reduction in the model at the bearings or elsewhere.

(c) As predicted by Yamamoto [16] and earlier
simulations [15], bearing clearances can drop
the peak-vibration *running* speed into the
operating range, and <u>these synchronous
vibration loads would appear to pose a more
serious threat to bearing lifetime than the
subsynchronous motion.</u>

The following options are being pursued to
improve the dynamic characteristics of the HPOTP:

(a) Units are being prepared for tests which
include a stiffened rotor, damper seals at
the boost impeller, and a modified turbine
interstage seal.

(b) Although attractive from a dynamics
viewpoint, the shrouded inducer design poses
serious manufacturing problems and also
raises concerns with respect to cavitation
performance. Pending resolution of these
problems, no test of this configuration are
presently scheduled.

Figure 13 illustrates simulation results for the
nominal nonlinear model with damper seals at 29,500
cpm. Observe the sharp reduction in synchronous
bearing loads. This reduction is due to (a) load
sharing by the seals and (b) increases in damping
which, according to Yamamoto's predictions, lower the
peak bearing reaction amplitudes. Figure 14
illustrates the bearing reaction above FPL. Observe
that clipping of the bearing loads due to motion in
and out of the deadband has actually increased. The
corresponding accelerometer spectrum is given in
figure 15, and demonstrates a rich spectrum of
subsynchronous components. The damper seals increase
bearing-reaction clipping by opposing the side load
and moving the rotor towards the center of the
bearing clearances. The model is setup with the seal
and bearing centers coincident radially. In an
actual engine, some lack of concentricity can be
expected which might counteract the seals centering
action.

An inspection of figures 13 trough 15 support the following conclusions with respect to implementation of the damper seals:

(a) In accordance with the linear predictions of figure 6, a marked reduction in synchronous bearing loads is predicted.

(b) Motion in and out of the bearing clearances is increased with a consequent increase in bearing-reaction-magnitude clipping and an increase in subsynchronous motion.

If current bearing distress is the result of excessive synchronous loads, seal modification should be very beneficial. However, if the bearing problems are associated with unloading and ball skidding, seal modifications will be counter-productive.

CONCLUSIONS

Linear and nonlinear analyses of the HPOTP support the following conclusions:

(a) By linear predictions, the second critical speed is only slightly above the FPL running speed and is lightly damped. Even a modest loss of bearing stiffness is sufficient to drop the second critical speed into the operating range and yield a prediction of excessive bearing loads.

(b) Based on prior test experience, the HPTOP appears to be lightly damped.

(c) The subsynchronous motion which is evident in test results can be obtained in a nonlinear model due to bearing clearances. Motion in and out of the deadband clearances excites subharmonic motion for a stable but lightly damped model.

(d) A whirl frequency of subsynchronous motion at 440 Hz is predicted by the nonlinear model which is consistent with test results but at odds with a linear prediction of 520 Hz.

This whirl frequency reduction results solely
from the bearing clearances, and does not
require any stiffness reduction in the model
at the bearings or elsewhere.

(e) Bearing clearances can drop the
peak-vibration running speed into the
operating range yielding a prediction of
excessive bearing loads.

(f) Incorporation of damper seals into the boost
impeller seals markedly reduces predicted
synchronous bearing loads, but increases
bearing-reaction clipping an subsynchronous
motion at FPL.

ACKNOWLEDGMENT

REFERENCES

1. Childs, D. W., "The Space Shuttle Main Engine High-Pressure Fuel Turbopump Rotordynamic Instability Problem," ASME Trans. J. of Engineering for Power, Vol. 100, January, 1978, pp. 48-57.

2. Beatty, R. F. and Rowan, B. F., "Determination of Ball Bearing Dynamic Stiffness," Proceedings, Second Workshop on Rotordynamic Instability Problems in High Performance Turbomachinery, NASA CP 2250.

3. Jones, A. B., "A General Theory for Elastically Constrained Ball and Radial Roller Bearings Under Arbitrary Load and Speed Conditions," ASME J. of Basic Engineering, Vol. 82, No. 2, June 1960, pp. 309-320.

4. Black, H. F., and Cochrane, E. A., "Leakage and Hybrid Bearing properties of Serrated Seals in Centrifugal Pumps," Paper G5, 6th International Conference in Fluid Sealing, Munich, German Federal Republic, 27 February - 2 March 1973.

5. Black, H. F., and Jensen, D. N., "Effects of High-Pressure Ring Seals on Pump Rotor Vibrations," ASME Paper No. 71-WA/FE-38, Winter Annual Meeting, Washington, D. C., 1971.

6. Black, H. F., Allaire, P. E., and Barrett, L. E., "The Effect of Inlet Flow Swirl on the Dynamic Coefficients of High-Pressure Annular Clearance Seals," Ninth International Conference on Fluid Sealing, BHRA Fluid Sealing Conference, Leeuwenhorst, The Netherlands, April 1981.

7. von Pragenau, G. L., "Damping Seals for Turbomachinery," NASA TP-1987, March 1983.

8. Childs, D. W. and Kim C-H., "Analysis and Testing for Rotordynamic Coefficients of Turbulent Annular Seals with Different, Directionally-Homogeneous Surface-Roughness Treatment for Rotor and Stator Elements," presented at the Third Rotordynamics Instability Workshop at Texas Texas A&M University, College Station, TX, May 28-30, 84.

9. Nelson, C. D., "The Rotordynamic Coefficients of High-Pressure Annular Gas seals," accepted for presentation at the 1984 ASME Gas Turbine Conference.

10. Thomas, J. J., "Instabilie Eigenschwingungen von Turbine Laufern, angefacht durch die Spaltstromungen Stopfbushsen un Beschaufelungen, AEG-Soderdruch, 1958.

11. Alford, J., "Protecting Turbomachinery From Self-Excited Rotor Whirl," ASME Trans. J. of Engineering for Power, October 1965, pp. 333-345.

12. Hauck, L., "Measurement and Evaluation of Swirl-Type Flow in Labyrinth Seals," NASA CP 2250 Rotordynamic Instability Problems in High-Performance Turbomachinery, Proceedings of a workshop held at Texas A&M University, 10-12 May 1982.

13. Chamieh, D. S., Acosta, A. J., Brennen, C. E., Caughey, T. K., and Franz, R., "Experimental Measurement of Hydrodynamic Stiffness Matrices for a Centrifugal Pump Impeller," NASA CP 2250 Rotordynamic Instability Problems in High Performance Turbomachinery, Proceedings of a workshop held at Texas A&M University, 10-12 May 1982.

14. Yamamoto, T., "On the Critical Speeds of a Shaft," Memoirs of the Faculty of Engineering, Nagoga University, Vol. 6, No. 2, 1954.

15. Childs, D. W., Rotordynamics Analysis for the HPOTP (High Pressure Oxygen Turbopump) of the SSME (Space Shuttle Main Engine), an Interim Progress Report for NASA Contract NAS8-31233, Dept. of Mechanical Engineering, The University of Louisville, 1979.
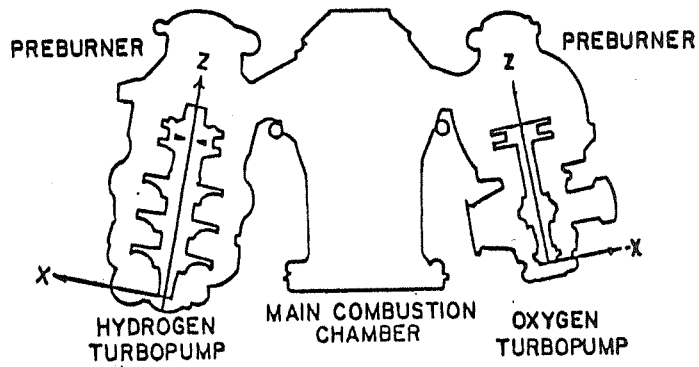
Figure 1. SSME powerhead component arrangement and local coordinate systems.
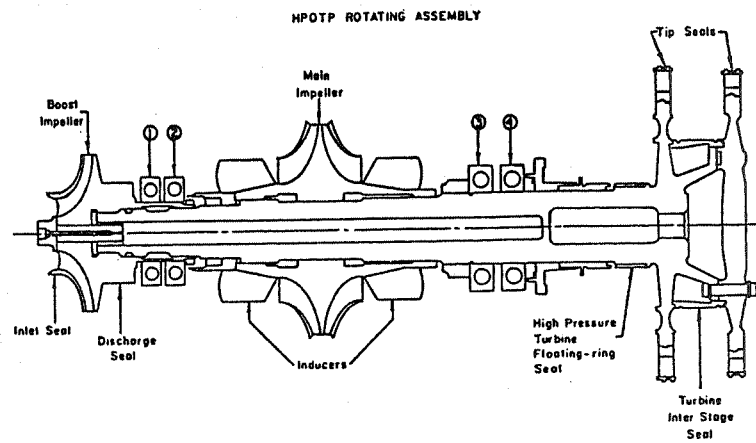
Figure 2. HPOTP rotating assembly.

STABILITY ANALYSIS SSME HPOTP
ω = 178.7 Hz. = 10725. RPM

STABILITY ANALYSIS SSME HPOTP
ω = 628.9 Hz. = 51751. RPM
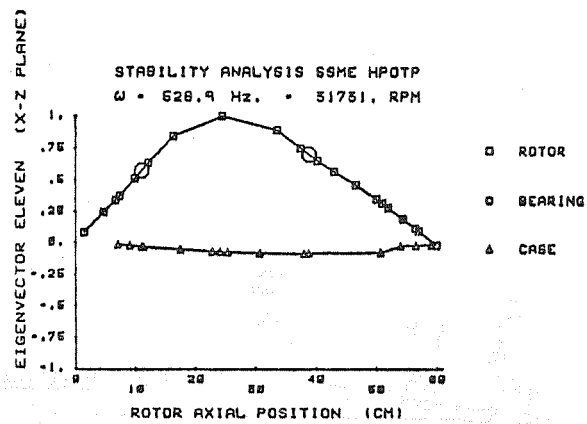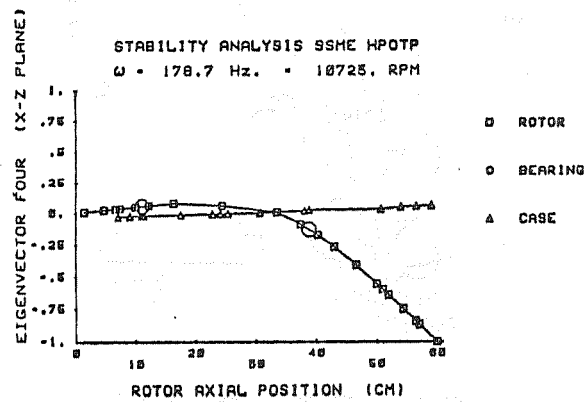
Figure 3. Undamped, zero-running-speed rotor-housing modes associated with the first and second critical speeds.

FREQUENCY RESPONSE ANALYSIS SSME HPOTP
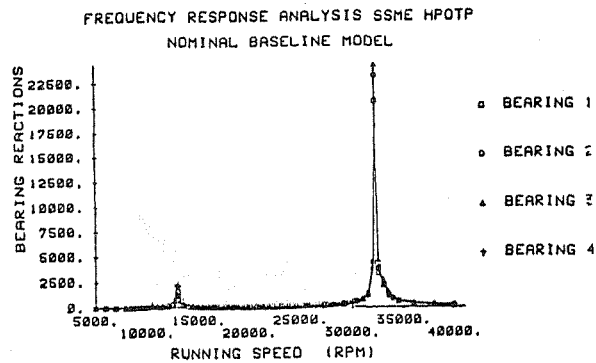NOMINAL BASELINE MODEL

Figure 4. Bearing reactions for the nominal linear
model with speeds out of 40,000 cpm.

FREQUENCY RESPONSE ANALYSIS SSME HPOTP
NOMINAL BASELINE MODEL
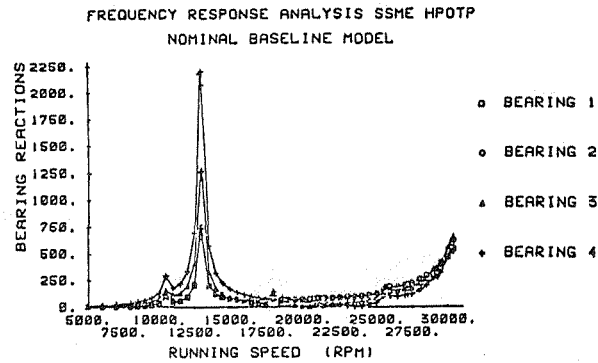
Figure 5 (a). Bearing reactions for the nominal linear
model for speeds from 5,000 cpm to FPL.

FREQUENCY RESPONSE ANALYSIS SSME HPOTP
NOMINAL BASELINE MODEL
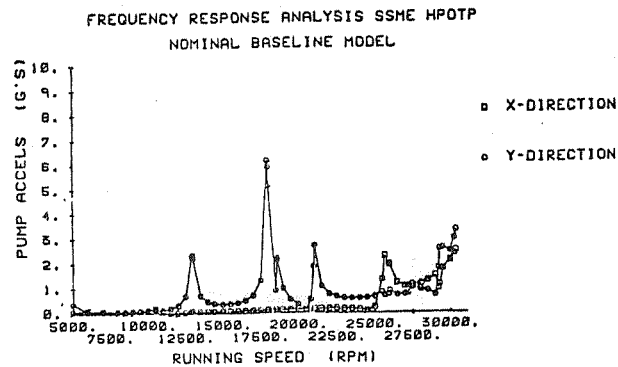
Figure 5 (b). Pump accelerometer levels in the X-Z
and Y-Z planes.

475

FREQUENCY RESPONSE ANALYSIS SSME HPOTP
NOMINAL BASELINE MODEL
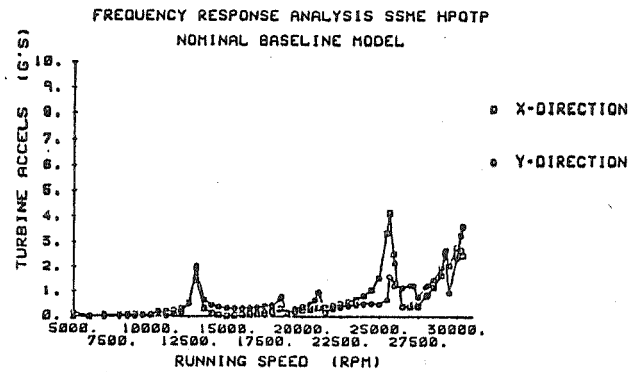
Figure 5 (c). Turbine accelerometer levels in the
X-Z and Y-Z planes.

FREQUENCY RESPONSE ANALYSIS SSME HPOTP
SMOOTH ROTOR - ROUGH HOUSING FWR & RWR
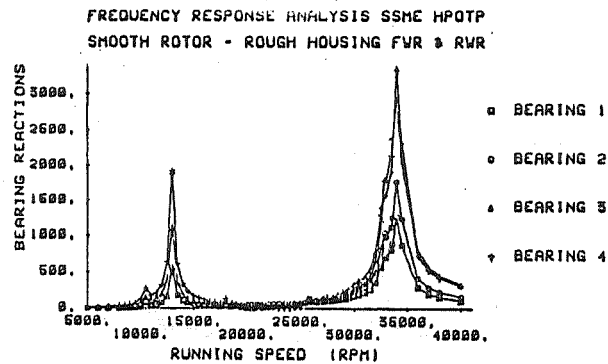
Figure 6. Bearing reactions for the nominal model
with "damper" seal coefficients for the
boost-impeller inlet and discharge seals.

FREQUENCY RESPONSE ANALYSIS SSME HPOTP
SHROUDED INDUCER SEALS
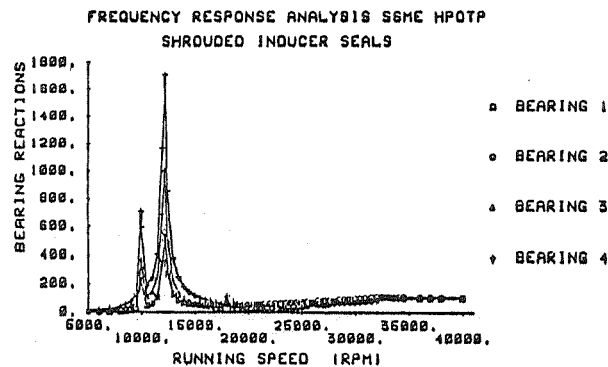
Figure 7. Bearing reactions for the model with seal
coefficients for a shrouded impeller.

476
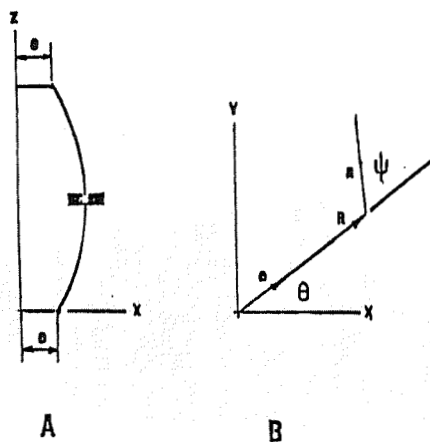
Figure 8. Yamamoto's model for synchronous response with bearing clearance.
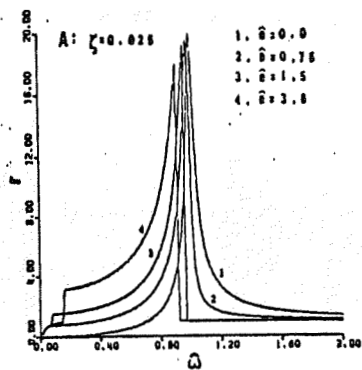
Figure 9. Synchronous-response characteristics for Yamamoto's model with increasing bearing clearances.

TRANSIENT ANALYSIS SSME HPOTP
STEADY STATE AT 30,381 RPM
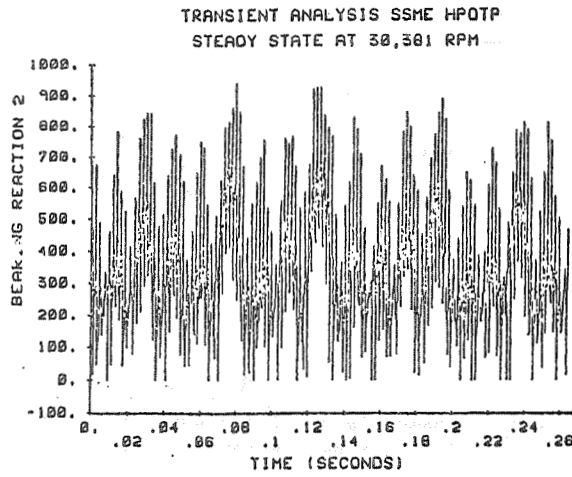
Figure 10 (a). Bearing 2 reaction magnitude versus
time at FPL for the nominal nonlinear
model.

TRANSIENT ANALYSIS SSME HPOTP
STEADY STATE AT 30,381 RPM
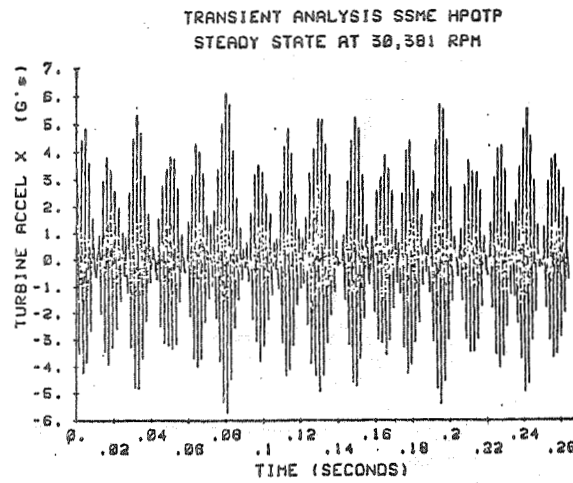
Figure 10 (b). Turbine X-Z plane acceleration
magnitude versus time for the
nominal nonlinear model.
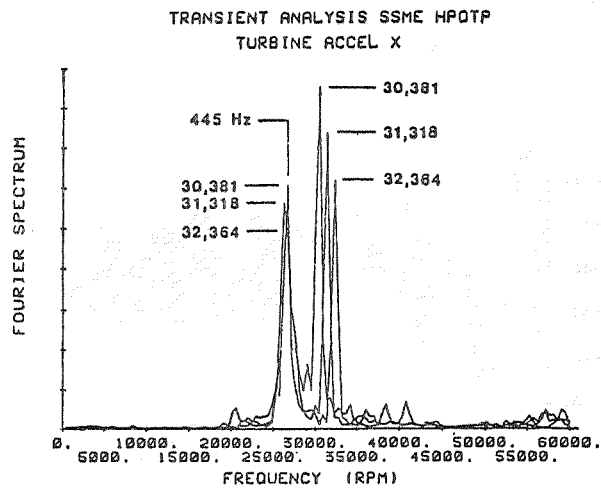
Figure 11. Turbine X-Z plane acceleration spectra
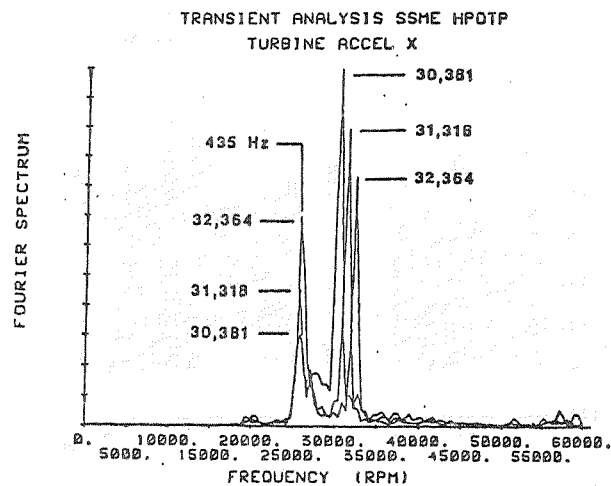at FPL and higher speeds for the nominal
nonlinear model.

Figure 12. Turbine X-Z plane acceleration spectra
at FPL and higher speeds for nonlinear
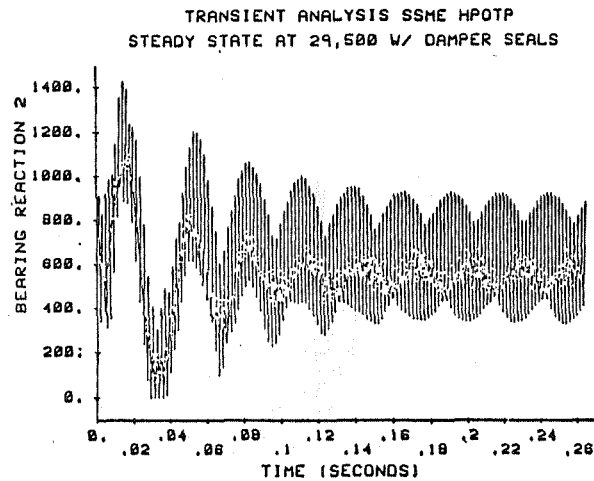model number 2.

479

TRANSIENT ANALYSIS SSME HPOTP
STEADY STATE AT 29,500 W/ DAMPER SEALS

Figure 13. Bearing 2 reaction magnitude at 29,500 cpm for the nominal nonlinear model with damper seals at the boost impeller.

TRANSIENT ANALYSIS SSME HPOTP
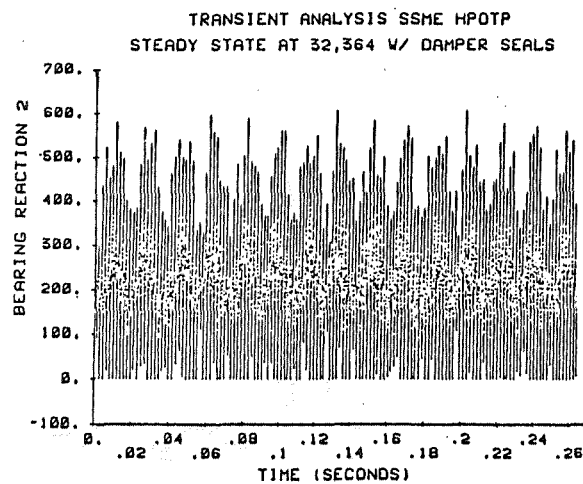STEADY STATE AT 32,364 W/ DAMPER SEALS

Figure 14. Bearing 2 reaction magnitude at above FPL for the nominal nonlinear model with damper seals at the boost impeller.

480

STEADY STATE AT 32,364 W/ DAMPER SEALS
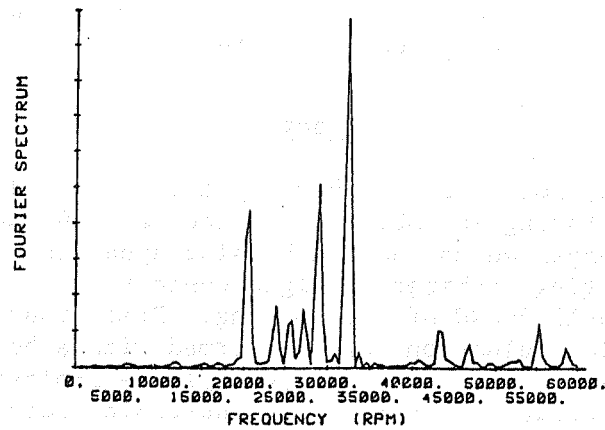PREBURNER ACCEL X

Figure 15. Preburner X-Z accelerometer spectrum at
            FPL for the nominal nonlinear model with
            damper seals at the boost impeller.

481